Geothermal Temperature and Pressure Transient Analyses of Well CHI-8A, El Salvador During Pressure Falloff

Jorge Alberto Rangel Arista[1]*, Sadiq J. Zarrouk[1], Eylem Kaya[1], and Roberto Enrique Renderos Pacheco[2]

[1]Department of Engineering Science, University of Auckland, Private Bag 90210, Auckland, New Zealand

[2] LAGEO Ltd., El Salvador

*jran489@aucklanduni.ac.nz

Keywords: *Geothermal, Temperature transient analysis, Pressure transient analysis, Temperature derivative, Well testing.*

ABSTRACT

Temperature transient analysis (TTA) examines the transient temperature logs of a well during completion testing. Most of the studies encompass only oil and gas reservoirs. The capabilities of geothermal temperature transient analysis have not been thoroughly studied. This paper examines the geothermal well CHI-8A, El Salvador, during pressure falloff. Two approaches were considered; analysis of pressure response (PTA); examination of temperature and pressure responses (TTA-PTA). By matching temperature and pressure, our study shows that geothermal TTA improves the resolution of geothermal PTA. Geothermal TTA complements geothermal PTA and provides further insight.

1. INTRODUCTION

The pressure transient analysis (PTA) examines pressure and flow rate data from well during well testing. Most PTA assumes constant fluid temperature (isothermal conditions) (Sidorova et al., 2014). Sometimes this assumption produces unconvincing results because it neglects the temperature effects (Benson and Bodvarsson, 1986; Zarrouk and McLean, 2019).

The temperature transient analysis (TTA) studies the temperature response during the well test (Rangel-Arista et al., 2023). TTA assumes non-isothermal conditions, making it ideal to complement PTA (Palabiyik et al., 2016; Ramazanov et al., 2010).

Onur et al. (2008) investigated PTA-TTA, utilising lumped parameter models for geothermal reservoirs. Palabiyik et al. (2016) introduced analytical equations considering PTA-TTA for early, intermediate and late times. Onur and Cinar (2016) proposed the temperature derivative expression (Equation 1), which uses shut-in time for calculations and produces absolute values.

$$abs\left(\Delta T'_{ln\,t}\right) = \left|\frac{d\Delta T}{d\,ln\,\Delta\,t}\right| \qquad (1)$$

Where T is the temperature ($°C$), and t is the time (s).

Panini and Onur (2018) proposed a PTA-TTA analytical model for a vertical oil well in a radial composite reservoir. Rangel-Arista et al. (2022) used a novel geothermal framework to analyse the temperature and pressure response to estimate parameters: skin factor, skin radius, skin permeability, and reservoir permeability.

Most PTA-TTA studies contemplate gas and oil reservoirs, considering geothermal reservoirs sporadically. This paper uses numerical modelling to compare geothermal PTA and PTA-TTA results during pressure falloff from well CHI-8A in El Salvador.

2. CASE OF STUDY: CHI-8A

Figure 1 shows the casing profile of geothermal well CHI-8A, a single-phase (only liquid) wellbore. The total depth is 1594.5 m.

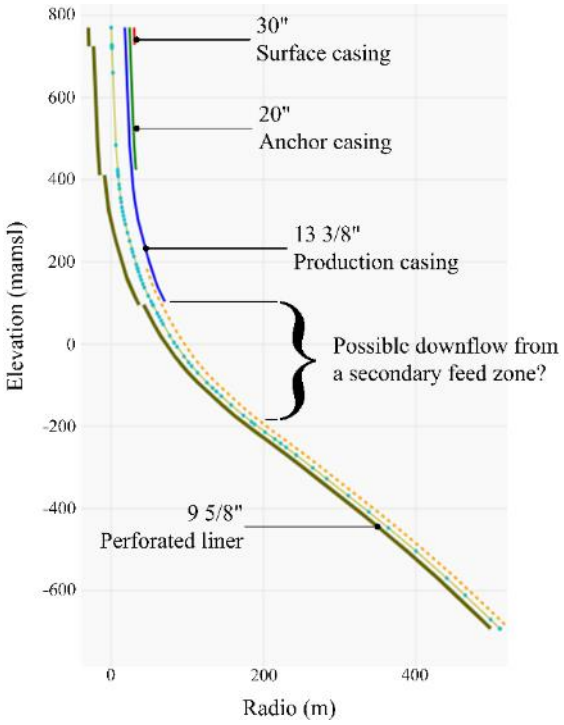

Figure 1: Casing diagram: Well CHI-8A.

Figure 2 shows the pressure, temperature, tool depth, and injection flow rate during well testing of CHI-8A. The test had two injection steps and one pressure falloff step. Throughout period A (Figure 2), fluid flow was zero. The sensor tool descended from the ground level to below 1000 m above the main feed zone. Pressure remained almost constant whilst temperature built up before the first injection step.

At period B (Figure 2), the injection fluid flowed at 18.6 L/s. Pressure built up from 46 to 56 bar. The downhole temperature tool recorded a short falloff followed by a slight buildup. Next, the temperature fell off throughout period B of water injection. These minor variations in temperature during injection result from the injection pump operation that is not as instant as presented in Figure 2.

ISSN 2703-4275

The second injection step (period C) used a flow rate of 32.8 L/s (Figure 2). The pressure went through another buildup period, reaching 65 bar. Temperature experienced a slight falloff and stabilised at around 43°C by the end of period C.

After the second injection step (Figure 2), the injection flow rate dropped to zero (period D). The pressure underwent a rapid falloff suffering a drop of almost 20 bar in less than ~1700 s (Figure 3), indicating good permeability (Zarrouk and McLean, 2019). The pressure stabilised around 46.5 bar. Then after ~6000 s, the pressure rebounded below 47 bar, probably because of a suspected downflow in the well (McLean et al., 2018; Zarrouk and McLean, 2019).

During pressure falloff (Figures 2-3), the temperature built up from 43°C to 100°C (period D). The temperature remained around 43°C during the first ~1300 s. Next, the temperature rise was significant until the end of the falloff.

After period D, the downhole tool (PT sensor) was moved upward along the well, with pressure and temperature dropping along the path (Figure 2). The highest temperature recorded was 110°C.

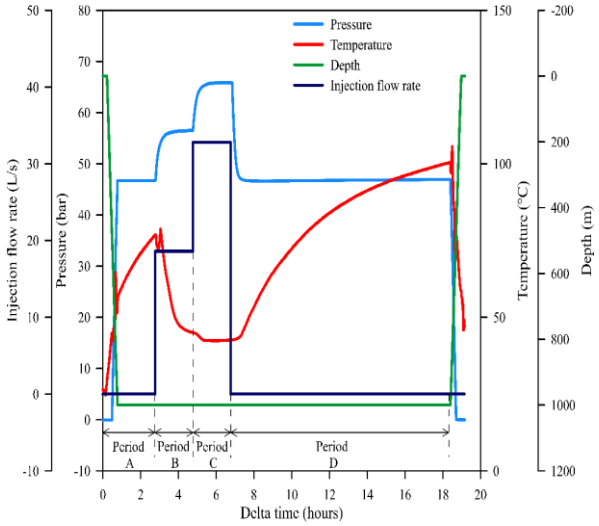

Figure 2: Injection/falloff test: CHI-8A well.

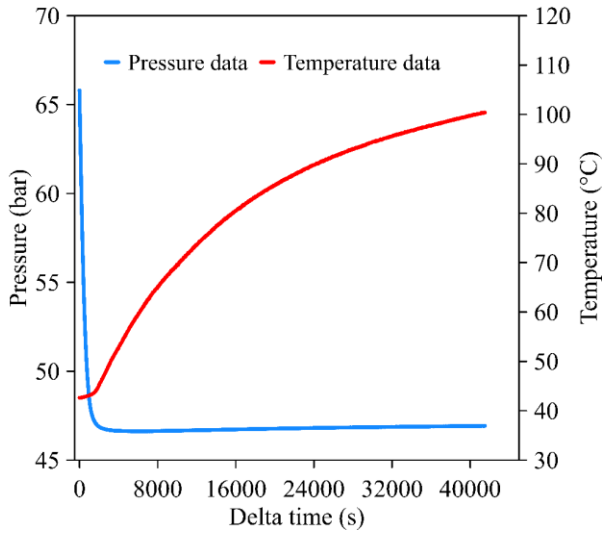

Figure 3: Temperature and pressure along falloff time (period D).

CHI-8A has a zero-wellhead pressure (WHP) during injection, indicating an infinity permeability well (Zarrouk and McLean, 2019; Rangel-Arista et al., 2023). Therefore, we calculated the injectivity index, resulting in 5.53 tonne/h/bar (Figure 4), using reservoir pressure to compare with other wells.

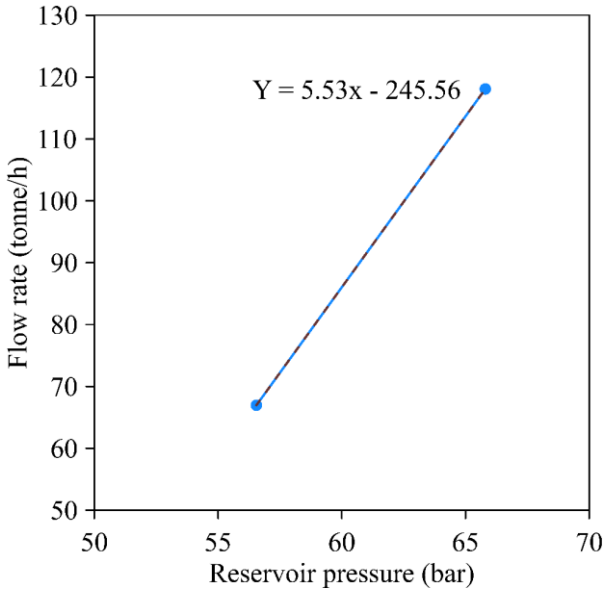

Figure 4: Injectivity Index: CHI-8A well.

3. FRAMEWORK SET-UP

We utilised the framework suggested by Rangel-Arista et al. (2022) for the numerical modelling of geothermal TTA-PTA. Rangel-Arista et al. (2022) framework was built upon McLean and Zarrouk's (2017) framework for geothermal PTA.

The grid geometry consists of three radial layers with multiple blocks in the radial direction (Figure 5) (Rangel-Arista et al., 2022). The blocks are spaced logarithmically, representing the wellbore, skin zone and reservoir. The central cylinder blocks represent the wellbore. Skin zone blocks can range from the wellbore radius up to 100 m. Reservoir blocks extend from the skin zone to 20000 m.

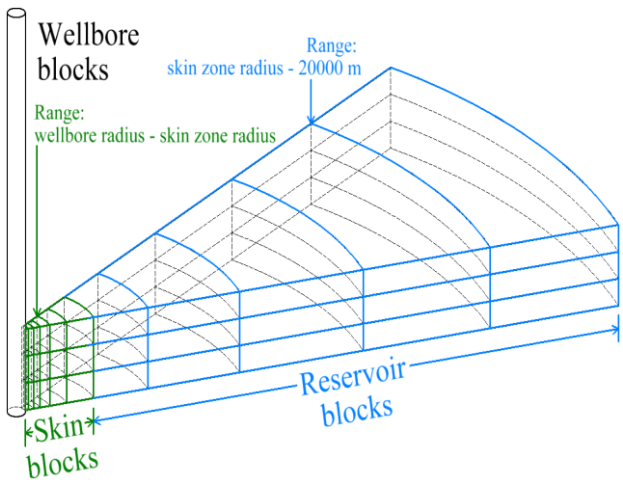

Figure 5: Geothermal TTA grid geometry.

ISSN2703-4275

The fractional dimension model (Zarrouk and McLean, 2019) was utilised to represent the fractured reservoir in dynamic conditions (Barker, 1988). This method simulates better complex fractured reservoirs without explicitly considering rock mechanics (Zarrouk et al., 2007).

The fractional dimension ranges from one to three, mainly containing non-integer values (fractional numbers). Number one represents a linear flow along a plane (fracture wall). Two represents radial flow converging in the well, forming a round disc. And three represents flow from all directions converging in the well, creating a spherical flow (Zarrouk and McLean, 2019).

The fractional dimension number modifies the volume of the blocks as well as the contact area between them. Table 1 shows the equations to modify the volume blocks and connection areas according to the number of fractions needed (O'Sullivan et al., 2005).

Table 1: Block volumes and connection areas expressions for the fractional dimension model.

Dimension of model	Block volumes	Connection areas
1	$2b^2\left(r_{i+1/2} - r_{i-1/2}\right)$	$2b^2$
2	$\pi b\left(r_{i+1/2}^2 - r_{i-1/2}^2\right)$	$2\pi b r_{i+1/2}$
3	$\left(\frac{4\pi}{3}\right)\left(r_{i+1/2}^3 - r_{i-1/2}^3\right)$	$4\pi r_{i+1/2}^2$
n	$\left(\frac{\alpha_n b^{3-n}}{n}\right)\left(r_{i+1/2}^n - r_{i-1/2}^n\right)$	$\alpha_n b^{3-n} r_{i+1/2}^{n-1}$

r: distance from the well; b: "thickness" of the fracture network; n: the dimension of model; $\alpha_n = 2\pi^{\frac{n}{2}}/\Gamma\left(\frac{n}{2}\right)$, Γ: gamma function.

The AUTOUGH 2.42 reservoir simulator was employed. It is based on TOUGH2 (Pruess, 2012), a general-purpose simulator to model subsurface fluid and heat flow in geothermal reservoirs.

PyTOUGH was utilised to control all the aspects of AUTOUGH 2.42: grid construction, data files, analysis of results, plots, initial conditions, boundary conditions, and physical parameters (Croucher, 2020).

Table 2 shows the parameters used for the geothermal PTA and TTA-PTA frameworks. Equation of State EOS1 is the option to simulate pure water in AUTOUGH 2.42. Wellbore volume, reservoir thickness, and wellbore radius are the values from well CHI-8A. The permeability in the wellbore blocks was three times higher than the reservoir permeability to avoid numerical convergence problems (Zarrouk and McLean, 2019). The skin zone and reservoir utilised 40 and 60 blocks per layer, respectively, resulting from our experiments to calibrate the geothermal TTA-PTA framework.

The Falloff time is divided into multiple steps to better match the pressure and temperature data. The fractional dimension number changes in each step (remaining parameters constant) to obtain the pressure match because the reservoir fracture network is dynamic along the injection and falloff times (pressure changes).

Table 2: Geothermal TTA-PTA and PTA frameworks parameters.

Parameter	Value
Equation of State (EOS)	EOS1
Well volume (m^3)	75.1
Reservoir thickness (m)	938.5
Well radius r_w (m)	0.122
Well permeability: order of magnitude greater than reservoir permeability k	3
Model radial extent (km)	20
Number of layers	3
Skin zone blocks per layer	40
Reservoir blocks per layer	60

The heat transfer (conduction, convection and advection) is assumed to be controlled by a hypothetical thermal diffusion coefficient. This assumption simplifies the complex heat transfer between the wellbore and reservoir throughout the feedzones. In these areas, hot and cold fluids enter and leave the well through a complex network of fractures within the reservoir. The full representation would require a complete map of all the feed zones containing each particular behaviour during well testing.

The hypothetical thermal diffusion coefficient is considered for wellbore and skin zone blocks, changing for each step to match the temperature response. The hypothetical thermal diffusion coefficient change indicates how fast or slow the heat is being transferred from the reservoir to the wellbore. Values of this parameter close to the actual thermal diffusion coefficient of the water indicate that most heat transfer is due to conduction. Consequently, the fluid is almost static. Higher values of this parameter denote convection, meaning a fluid flow from the reservoir to the well exists.

Table 3 shows the realistic thermal diffusion coefficients of the wellbore, skin zone and reservoir. The thermal properties of the liquid water were calculated using the equations provided by the International Association for the Properties of Water and Steam (IAPWS, 2018; IAPWS, 2008). The thermal properties of the reservoir rock are obtained from Somerton (1992).

Table 3: Thermal properties of well, skin zone, and reservoir.

Zone	Thermal conductivity (W/m·K)	Density (kg/m^3)	Specific heat (J/kg·K)	Thermal diffusivity (m^2/s)
Well	1.0	900.0	4500.0	2.4×10^{-7}
Skin	3.0	2500.0	900.0	13.3×10^{-7}
Reservoir	3.0	2500.0	900.0	13.3×10^{-7}

ISSN2703-4275

4. RESULTS

4.1. Pressure and temperature matches

We considered two models. The first model matched pressure and pressure derivative responses using only fractional dimension numbers (PTA). The second model matches the pressure, pressure derivative and temperature responses (TTA-PTA). The second model utilised the fractional dimension numbers and hypothetical thermal diffusion coefficients for the well and skin zone. Additionally, we assumed a downflow of 2 L/s around ~1800 s after the falloff started for both cases because of the pressure rebound (Figure 3).

Figure 6 shows the first model results: pressure match and fractional dimension number. The pressure model matches the pressure data smoothly and consistently throughout the falloff period.

The fractional dimension starts around 1.2 (Figure 6), indicating that the fluid movement tends to flow along a plane (slot) from the reservoir to the wellbore. Suddenly, increases in the following steps above 1.5 (Figure 6). The increase of fractional number denotes a change in the fluid flow tendency from linear to radial (round disc).

Finally, the fractional number decreases continuously and stabilises around 1.1 (Figure 6). Fluid flow is primarily linear, indicating good permeability in the formation (Rangel-Arista et al., 2023).

Although the first model neglects the temperature match, the model follows the temperature data trend (Figure 6). The temperature model reached above 80°C at the end of the falloff time.

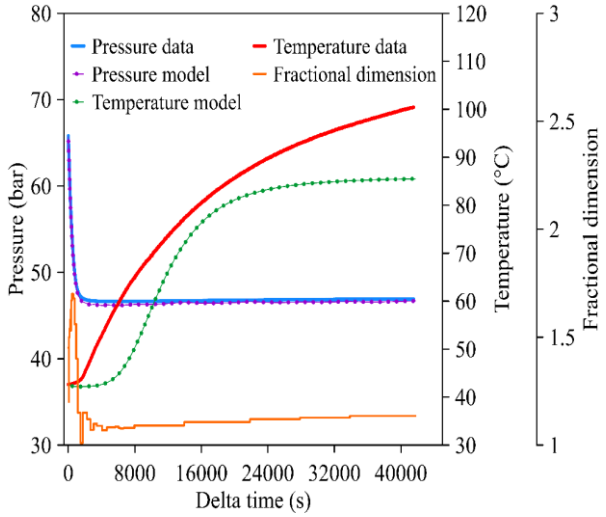

Figure 6: Pressure match and fractional dimension number, first case.

Figure 7 shows the pressure and temperature match for the second model. The pressure match improved compared to the first model, achieving a smoother match. The fractional dimension remains practically unchanged. The temperature model matches temperature data throughout all of the falloff time.

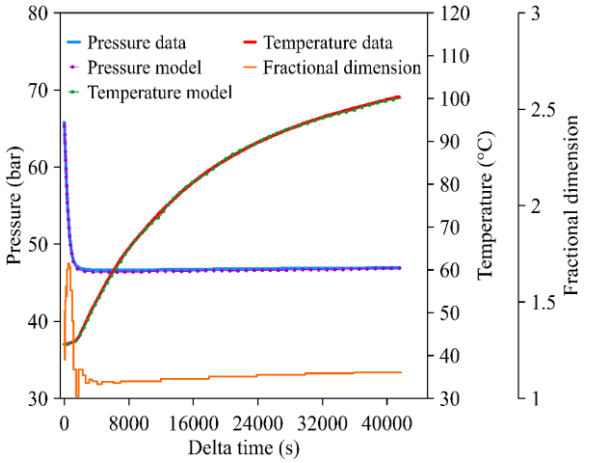

Figure 7: Pressure and temperature matches, second case.

Figure 8 shows the variation of the thermal diffusion coefficients (hypothetical) for the well and skin zone to attain the temperature match for the second case. Both coefficients (well and skin zone) are below the real coefficients in the first seconds because the temperature is still stabilising from the injection step. Suddenly, both coefficients increase briefly and fall (~300 s), denoting that convection is the primary heat transfer mechanism in these first moments when the mixture of cold fluid (injected fluid) and hot fluid is still taking place (flow condition).

Then, the coefficients increase slightly, maintaining the trend until around ~1300 s (Figure 8). During this short period, the temperature remains at almost 43°C, denoting that conduction drives heat transfer (no-flow condition).

Next, both coefficients increase at a higher rate, around ~1300 s (Figure 8), meaning that hot fluid comes into the well from the reservoir. Convection is the predominant heat transfer mechanism (flow condition). The temperature trend changes (`kick in`), and the temperature starts to rise faster.

After this `kick in` in the temperature (Figure 8), the coefficients (hypothetical well and skin thermal diffusivities) increase continuously throughout the falloff period. The temperature rises over time, reaching a temperature above 100°C. Throughout this time, convection remains.

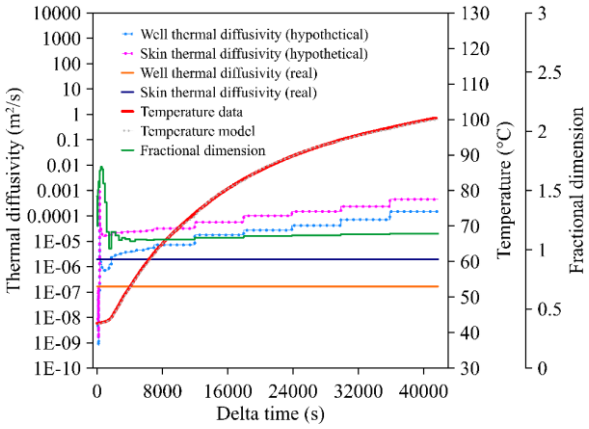

Figure 8: Temperature match and thermal diffusion coefficients, second case.

ISSN2703-4275

Figure 9 compares the two fractional dimension numbers for the first (PTA) and second (TTA-PTA) cases. The variation between numbers is slight. The most appreciable difference occurs around ~14000 s. Both numbers reaffirm the presence of high permeability (Rangel-Arista et al., 2023).

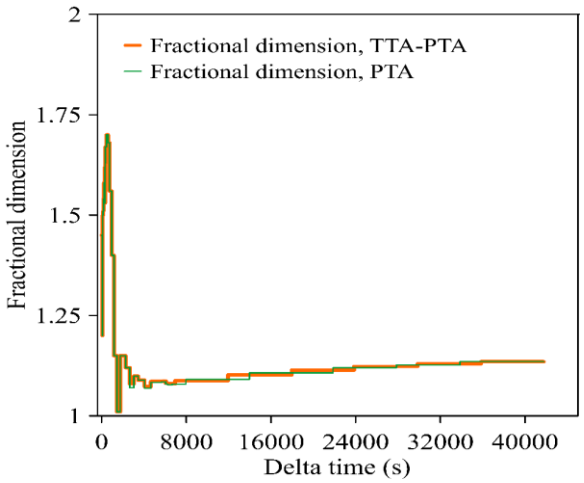

Figure 9: Fractional dimension comparison between first (PTA) and second (TTA-PTA) cases.

4.2. Pressure and pressure derivative.

4.2.1. Pressure

Figure 10 shows the delta pressure (dP), and pressure derivative (dP') match for the first model. The match for both is reasonable, following the correct trend.

The unit slope matches the beginning of the pressure derivative (Figure 10), showing the wellbore storage effect (~60 s). Then the characteristic pressure derivative hump appears without an infinite acting radial flow.

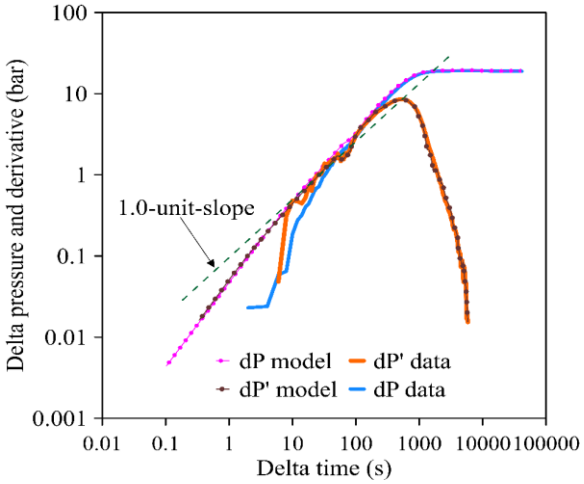

Figure 10: Delta pressure (dP) and pressure derivative (dP'), first model (PTA only).

For the second model, we can see in Figure 11 that including temperature matching improves pressure matching. The pressure derivative (dP') and delta pressure (dP) present a smoother match during the pressure falloff period.

4.2.2. Temperature

We computed the temperature derivative employing the shut-in time (Onur and Cinar, 2016) and the superposition time for pressure (Equation 2) (Houze et al., 2016).

$$S_n(\Delta t) = \sum_{i=1}^{n-1} \frac{q_i - q_{i-1}}{q_n - q_{n-1}} log(t_n - t_i + \Delta t) + log\, \Delta\, t \quad (2)$$

Where S_n is the superposition function of time for pressure, $q_{i,i-1}$ is the flow rate during the ith or ith-1 rate period in a variable-rate test (m^3/s), $q_{n,n-1}$ is the flow rate during the nth or nth-1 rate period in a variable-rate test (m^3/s), t_n is the time during nth rate period in a variable-rate test (s), and t_i is the time during ith rate period in a variable-rate test (s).

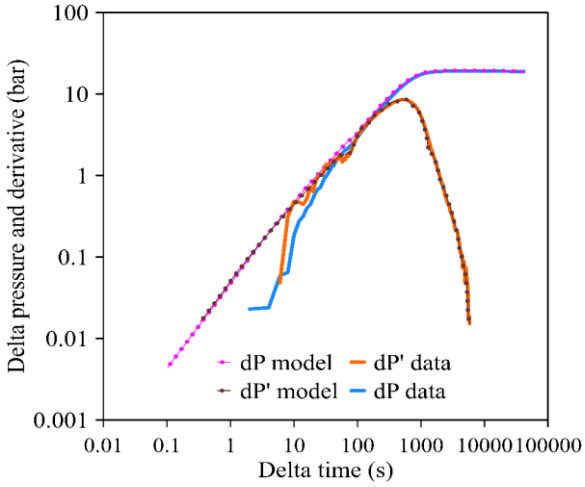

Figure 11: Delta pressure (dP) and pressure derivative (dP'), second case.

Figure 12 compares the temperature derivative using shut-in time (dT' Sit) and superposition time for pressure (dT' Spt). Both derivatives employed the actual temperature data during the falloff time.

The derivative trends are similar, showing the most relevant difference at the end (Figure 12). The shut-in time (dT' Sit) produces a flatter curve than the superposition time after 1000 s.

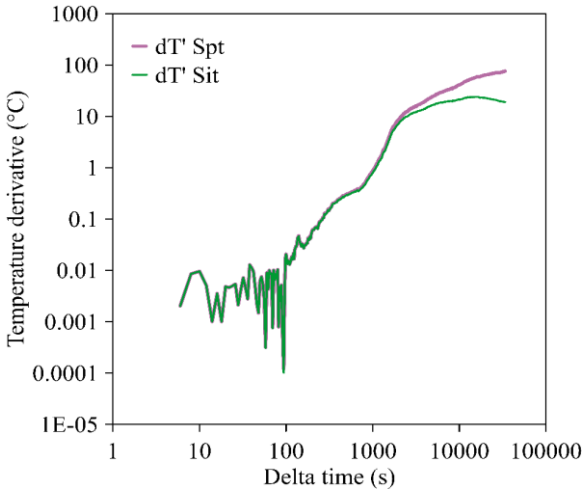

Figure 12: Temperature derivative using shut-in time (dT' Sit) and superposition time for pressure (dT' Spt), considering the actual temperature.

ISSN2703-4275

Figures 13 and 14 show the temperature derivative match utilising the superposition time for pressure for the first and second cases. Considering the temperature match (second case, Figure 14) produces a better temperature derivative match than neglecting it (first model, Figure 13). Although considering temperature yields a better match, the first 100 s is challenging because brief fluctuations produce peaks tending to zero. These peaks might be related to the wellbore storage effect because the temperature remains almost constant, indicating the absence of fluid flow from the skin zone and reservoir.

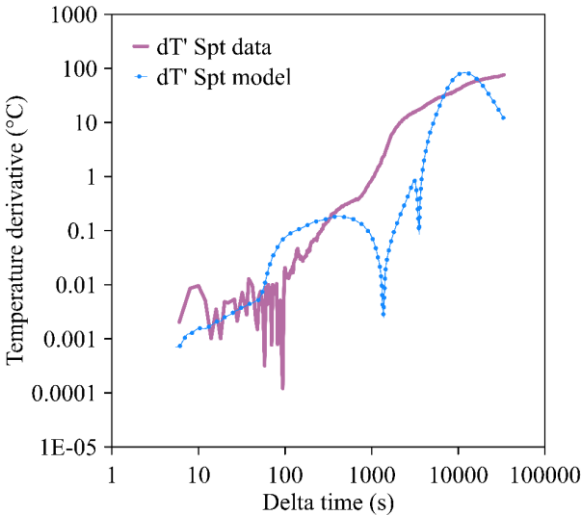

Figure 13: Data (dT' Spt data) and model (dT' Spt model) temperature derivatives using superposition time for pressure, first case.

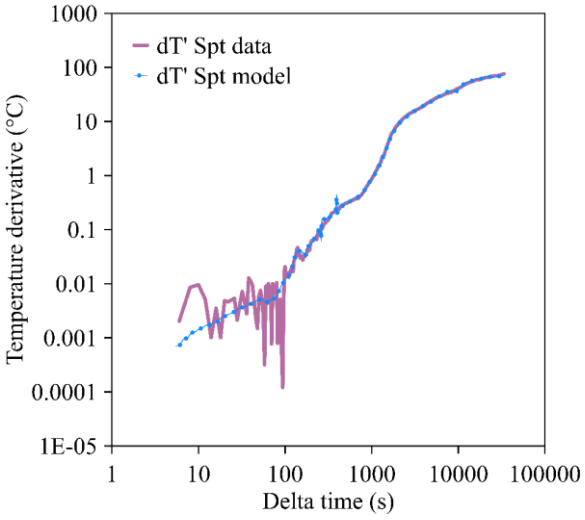

Figure 14: Data (dT' Spt data) and model (dT' Spt model) temperature derivatives using superposition time for pressure, second case.

Temperature derivatives employing the shut-in time (Figures 15 and 16) show a similar pattern to superposition time for pressure (Figures 13 and 14). The trends are analogous, regardless of the pressure or temperature matches.

4.3. Radial temperature response

Figure 17 shows the radial temperature contour after the second injection stopped. The temperature gradient extends only one meter away from the central axis of the wellbore. This perturbation might indicate that the temperature transient analysis is associated more with the wellbore and skin zone because the perturbation is unable to reach deeper distances into the reservoir.

4.4. Estimation of parameters

Table 4 compares the results for the first and second models. The first model considers only pressure and pressure derivative matches (PTA). The second case adds temperature the match (TTA-PTA).

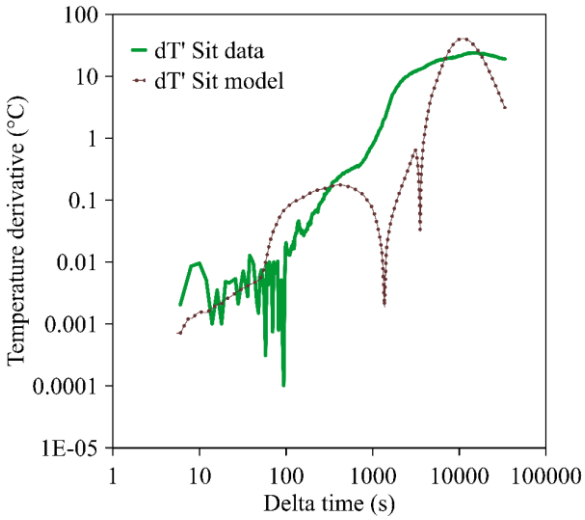

Figure 15: Data (dT' Sit data) and model (dT' Sit model) temperature derivatives using shut-in time, first model.

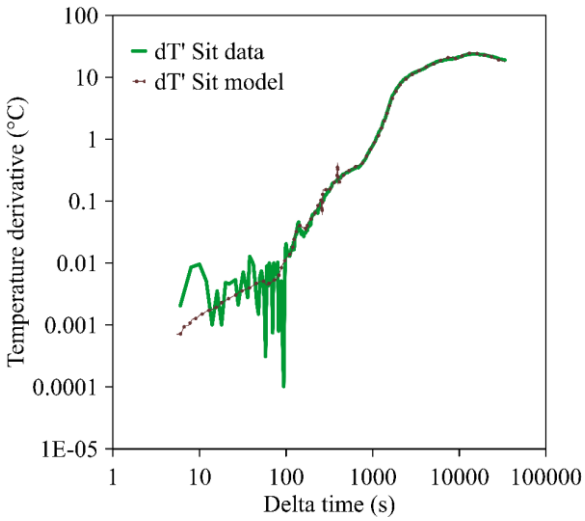

Figure 16: Data (dT' Sit data) and model (dT' Sit model) temperature derivatives using shut-in time, second model.

The estimated parameters are nearly the same values for both models (Table 2). We can notice a slight difference in the skin radius, skin factor and reservoir permeability. The most considerable difference is the skin zone permeability because the skin zone radius considering PTA is one meter less than the skin zone radius considering PTA-TTA.

ISSN2703-4275

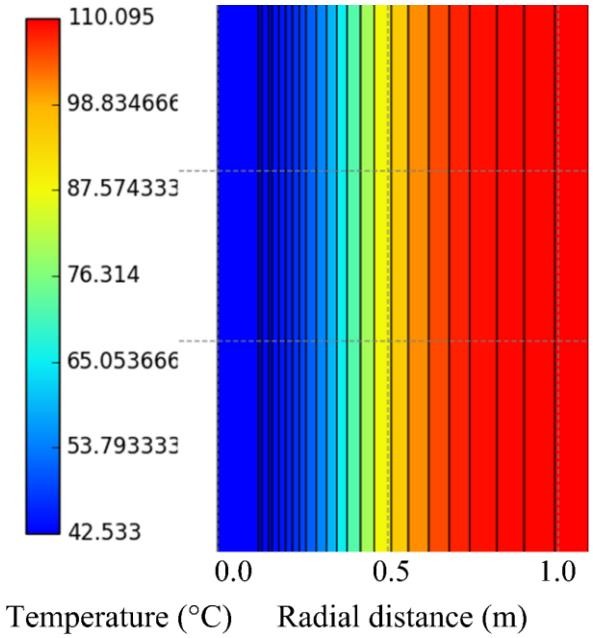

Figure 17: Radial temperature contour after the second fluid injection step.

Table 4: Estimation of parameters for the first and second cases.

Parameters	PTA	PTA-TTA
Injectate temperature: T_{inj} (°C)	43.3	43.3
Reservoir permeability: k x10^{-15} (m^2)	111	110
Skinfactor: s (dimensionless)	-3.55	-3.5
Skin zone permeability: k_s x10^{-15} (m^2)	2525	1083
Reservoir thickness: h (m)	938.50	938.50
Skin zone radius: r_s (m)	5	6
Well radius: r_w (m)	0.122	0.122

5. CONCLUSIONS

The consideration of geothermal TTA improves the resolution of geothermal PTA. Therefore, geothermal TTA complements geothermal PTA.

CHI-8A shows good permeability in the skin and reservoir zones. The pressure underwent a rapid falloff suffering a drop of almost 20 bar in less than ~1700 s, indicating good permeability.

The hypothetical thermal diffusion coefficient assumption proved to be useful to match the temperature response and simplify the complex heat transfer within the wellbore (where the PT tool is located).

As shown in Figure 8, the hypothetical thermal diffusivity increases gradually with time to match the fast increase in wellbore temperature during pressure falloff; this confirms the downflow of hotter fluid from upper formations down the wellbore into the more permeable loss zone.

We feel that using numerical TTA along with the numerical PTA framework will help better estimate the reservoir parameters and enhance our understanding of the complex geothermal reservoir conditions. This will effectively lead to a better geothermal well-test interpretation using already available transient temperature data that usually are ignored.

ACKNOWLEDGEMENTS

The authors thank Roberto Enrique Renderos Pacheco, Jose Luis Henriquez, and Elizabeth Torio Henriquez of LAGEO Ltd. El Salvador for kindly providing the field data.

The first author thanks the National Council of Science and Technology of Mexico (CONACYT) for kindly providing the PhD scholarship to study at the University of Auckland.

REFERENCES

Barker, J.A.: A generalised radial flow model for hydraulic tests in fractured rock. *Journal of Water Resources Research*. pp. 1796–1804. (1988).

Benson, S.M., Bodvarsson, G.S.: Non-isothermal Effects During Injection and Falloff Tests. *Journal of SPE (Society of Petroleum Engineers) Format. Eval. 1986*, USA. pp. 53-63. (1986).

Croucher, A.: PyTOUGH user's guide. Department of Engineering Science, University of Auckland. (2020).

Houzé, O., Viturat, D., Fjaere, O. S., Trin, S., Allain, O., Tauzin, E. (2011). Dynamic data analysis: The theory and practice of pressure transient, production analysis, well performance analysis, production logging and the use of permanent downhole gauge data. KAPPA. https://www.kappaeng.com/papers

IAPWS. (2018). Revised Release on the IAPWS Formulation 1995 for the Thermodynamic Properties of Ordinary Water Substance for General and Scientific Use. The International Association for the Properties of Water and Steam. http://www.iapws.org/release.html

IAPWS. (2008). Release on the IAPWS formulation 2008 for the viscosity of ordinary water substance. The International Association for the Properties of Water and Steam. http://www.iapws.org/release.html

Mclean, K., Zarrouk, S.: Pressure transient analysis of geothermal wells: A framework for numerical modelling. *Journal of Renewable Energy 2017*. pp. 737-746.

McLean, K., McDowell, J., Sepulveda, F., Seastres, J., Zarrouk, S. J., & Alcaraz, S. (2018, November). Upflow along a basement fault revealed by geothermal numerical pressure transient analysis. In *Proceedings 40th New Zealand Geothermal Workshop* (Vol. 14, p. 16).

Onur, M., & Cinar, M. (2016, May 30-June 2). Analysis of sandface-temperature-transient data for slightly compressible, single-phase reservoirs [Paper presentation*]. SPE Europec featured at the 78th EAGE Conference and Exhibition*, Vienna, Austria.

Onur, M., Sarak, H., Tureyen, O.I., Cinar, M., Satman, A.: A new non-isothermal lumped-parameter model for low

temperature, liquid dominated geothermal reservoirs and its applications. *Proc. Thirty-Third Workshop on Geothermal Reservoir Engineering Stanford University 2008*, California, USA. (2008).

O'Sullivan, M.J., Croucher, A.E., Anderson, E.B., Kikuchic, T., Nakagomed, O.: An Automated Well-Test Analysis System (AWTAS). *Journal of Geothermics*. pp. 3–25. (2005).

Palabiyik, Y., Onur, M., Tureyen, O.I., Cinar, M.: Transient temperature behaviour and analysis of single-phase liquid-water geothermal reservoirs during drawdown and buildup tests: Part I. Theory, new analytical and approximate solutions. *Journal of Petroleum Science and Engineering 2016*. pp. 637-656. (2016).

Panini, F., Onur, M.: Parameter Estimation from Sandface Drawdown Temperature Transient Data in the Presence of a Skin Zone Near the Wellbore. *Proc. the SPE Europec featured at 80th EAGE Conference and Exhibition 2018*, Copenhagen, Denmark. (2018).

Pruess, K. TOUGH2 User's Guide, Version 2, Earth Sciences Division, Lawrence Berkeley National Laboratory University of California, Berkeley, California (2012)

Ramazanov, A.Sh., Valiullin, R.A., Sadretdinov, A.A., Shako, V.V., Pimenov, V.P., Fedorov, V.N.: Thermal Modeling for Characterisation of Near Wellbore Zone and Zonal Allocation. *Proc. 2010 SPE Russian Oil & Gas Technical Conference and Exhibition 2010*, Moscow, Russia. (2010).

Rangel-Arista, J.A., Zarrouk, S.J., Kaya E. (2023). Temperature Transient Analysis in a Highly Fractured Geothermal Reservoir: An Updated Numerical Modelling Framework [Geothermics in press].

Rangel-Arista, J.A., Zarrouk, S.J., Kaya, E., McLean, K. (2022, November 23-25). Exploring the Use of Temperature Transient Analysis During Pressure Falloff Testing in Geothermal Wells [Paper presentation]. *44th New Zealand Geothermal Workshop, Auckland, New Zealand.*

Sidorova, M., Theuveny, B., Pimenov, V., Shako, V., & Guzman-Garcia, A.G. (2014, November 12–14). Do Not Let Temperature Transients Hinder Your Buildup Pressure Interpretation–Proper Gauge Placement in Highly Productive Reservoirs in Well Testing Operations [Paper presentation]. *In SPE Annual Caspian Technical Conference and Exhibition*, Astana, Kazakhstan. https://doi.org/10.2118/172278-MS

Somerton, W.H. (1992). Thermal properties and temperature-related behavior of rock/fluid systems. Elsevier. https://www.sciencedirect.com/bookseries/developments-in-petroleum-science/vol/37/suppl/C

Zarrouk, S., O'Sullivan, M., Croucher, A., Mannington, W.: Numerical modelling of production from the Poihipi dry steam zone: Wairakei geothermal system, New Zealand. *Journal of Geothermics 2007*. pp 289–303. (2007).

Zarrouk, S.J., McLean, K. (2019). Geothermal well test analysis: fundamentals, applications and advanced techniques. Elsevier. https://doi.org/10.1016/C2017-0-02723-4